NUCLEAR SCIENCE AND ENGINEERING · VOLUME 185 · 000–000 · JANUARY 2017

A High-Order Low-Order Algorithm with Exponentially Convergent Monte Carlo for Thermal Radiative Transfer

Simon R. Bolding,[a] Jim E. Morel,[a]* and Mathew A. Cleveland[b]

[a]*Texas A&M University, Department of Nuclear Engineering, College Station, Texas 77843*
[b]*Los Alamos National Laboratory, Los Alamos, New Mexico 87545*

Received January 31, 2016
Accepted for Publication May 24, 2016
http://dx.doi.org/10.13182/NSE16-36

Abstract — *We have implemented a new high-order low-order (HOLO) algorithm for solving thermal radiative transfer problems. The low-order (LO) system is based on the spatial and angular moments of the transport equation and a linear-discontinuous finite-element spatial representation, producing equations similar to the standard S_2 equations. The LO solver is fully implicit in time and efficiently resolves the nonlinear temperature dependence at each time step. The high-order (HO) solver utilizes exponentially convergent Monte Carlo (ECMC) to give a globally accurate solution for the angular intensity to a fixed-source pure-absorber transport problem. This global solution is used to compute consistency terms, which require the HO and LO solutions to converge toward the same solution. The use of ECMC allows for the efficient reduction of statistical noise in the Monte Carlo solution, reducing inaccuracies introduced through the LO consistency terms. We compare results with an implicit Monte Carlo code for one-dimensional gray test problems and demonstrate the efficiency of ECMC over standard Monte Carlo in this HOLO algorithm.*

Keywords — *Hybrid Monte Carlo, residual Monte Carlo, thermal radiative transfer.*

Note — *Some figures may be in color only in the electronic version.*

I. INTRODUCTION

We have implemented a high-order low-order (HOLO) algorithm for the one-dimensional (1-D) gray thermal radiative transfer (TRT) problems. The governing equations are the radiation and material energy balance equations, i.e.,

$$\frac{1}{c}\frac{\partial I(x,\mu,t)}{\partial t} + \mu\frac{\partial I(x,\mu,t)}{\partial x} + \sigma_t I(x,\mu,t) = \frac{\sigma_s}{2}\phi(x,t) + \frac{1}{2}\sigma_a acT^4(x,t) \quad (1)$$

and

$$\rho c_v \frac{\partial T(x,t)}{\partial t} = \sigma_a \phi(x,t) - \sigma_a acT^4(x,t)\,, \quad (2)$$

where

x = position
t = time
μ = x-direction cosine of the angular intensity $I(x,\mu,t)$
a = radiation constant
c = speed of light
ρ = mass density
c_v = specific heat
σ_a, σ_s, and σ_t = absorption, scattering, and total cross sections (cm^{-1}), respectively.

The desired unknowns are the material temperature $T(x,t)$ and the scalar radiation intensity $\phi(x,t) = \int_{-1}^{1} I(x,\mu,t)d\mu$. The

*E-mail: morel@tamu.edu

scalar intensity is related to the radiation energy density E by the relation $E = \phi/c$. The equations are strongly coupled through the gray Planckian emission source $\sigma_a acT^4$, which is a nonlinear function of temperature, and the absorption term $\sigma_a\phi$. In general, the material properties are a function of T. The temperature-dependent material properties and absorption and reemission physics lead to systems that require a solution in a mix of streaming and optically thick, diffusive regions.

A Monte Carlo (MC) solution to the TRT equations is typically achieved by the implicit Monte Carlo (IMC) method.[1] This method partially linearizes Eqs. (1) and (2) over a discrete time step, with material properties evaluated at the previous temperature. Linearization of the system produces a transport equation that contains an approximate emission source and an effective scattering cross section representing absorption and reemission of photons over a time step. This transport equation is advanced over a time step via MC. The MC simulation tallies energy absorption over a discretized spatial mesh. The energy absorption in each mesh cell is used to directly estimate a new end-of-time-step temperature in that cell. In optically thick regions, or for large time steps, the effective scattering dominates interactions. In these diffusive regions, IMC becomes computationally expensive. Acceleration methods typically attempt to improve efficiency by allowing particles to take discrete steps through optically thick regions based on a discretized diffusion approximation.[2,3] In IMC, the approximate linearization of the emission source is not iterated on within a time step due to the large computational cost of the MC transport each time step; this imposes a limit on the time-step size to produce physically accurate results.[4]

In IMC, the material and radiation energy fields are discretized spatially to solve for cell-averaged values. An inaccurate spatial representation of the emission source over a cell can result in energy propagating through the domain artificially fast, yielding nonphysical results referred to as the teleportation error.[5] The IMC method uses a fixup known as source tilting to mitigate this problem. Source tilting reconstructs a more accurate linear-discontinuous (LD) representation of the emission source within a cell based on the cell-averaged material temperatures in adjacent cells.

Moment-based hybrid MC methods provide an alternative solution method. Recent work has focused on so-called HOLO approaches.[6–9] Such methods utilize a low-order (LO) operator based on angular moments of the transport equation, formulated over a fixed spatial mesh. Physics operators that are time-consuming for MC to resolve, e.g., absorption-reemission and physical scattering events, are moved to the LO system. Newton methods allow for nonlinearities in the LO equations to be fully resolved efficiently.[6] The high-order (HO) transport equation is defined by Eq. (1), with sources that are truly implicit in time estimated from the LO solution. The HO equation is solved via MC to produce a high-fidelity solution for the angular intensity. The MC estimate of the angular intensity is used to estimate consistency terms, present in the LO equations, that require the LO system to preserve the angular accuracy of the MC solution. The HO system does not directly estimate a new material temperature, eliminating stability issues that require linearization of the emission source.

Sufficient MC histories must be performed to eliminate statistical noise in the consistency terms that can contaminate the LO solution. Exponentially convergent Monte Carlo (ECMC) (Refs. 9 and 10) provides an algorithm that can efficiently reduce statistical noise to the same order as the HOLO iteration error with significantly less particle histories than standard Monte Carlo (SMC). In particular, ECMC is exceptionally efficient in time-dependent TRT problems because information about the intensity from the previous time step can be used as an accurate initial guess for the new end-of-time-step intensity. Additionally, no particle histories are required in regions where the radiation and material energy field are in equilibrium, similar to Ref. 8. However, implementation of ECMC is nontrivial, requiring a finite-element (FE) representation of the solution in all phase-space variables that are being sampled with MC. The fundamental transport of particles is the same as SMC transport codes, but the source will now contain positive- and negative-weight particles.

Our ECMC solver contains similarities to the residual Monte Carlo (RMC) HO solver in Ref. 8, with some key differences. The RMC algorithm uses a particular, fixed estimate of the solution to significantly reduce the statistical noise in the simulation compared to a SMC simulation. The guess for the solution is chosen to produce only sources on the faces of cells, reducing the dimension of the phase space to be sampled.[8] The RMC algorithm uses a piecewise constant trial space representation for the intensity in x and μ. The primary difference between the methods is that ECMC iteratively estimates the solution, in batches, producing a known MC estimate of the error in that estimate. The ECMC algorithm projects the intensity onto a linear-discontinuous finite-element (LDFE) trial space, although the RMC algorithm could similarly be formulated with an LDFE representation. Adaptive mesh refinement (AMR) can be used in ECMC to produce highly accurate solutions with minimal statistical noise, as

long as sufficient particle histories are performed. The formulation of the residual in Ref. 8 uses an estimate of the solution such that only face sources need to be sampled. This residual formulation can produce minimal statistical noise in slowly varying problems where the behavior of the system is near equilibrium. Our ECMC algorithm has similar statistical efficiency by choosing the previous time-step intensity as the initial guess to the algorithm; however, a linear volumetric source must be sampled in addition to face sources. The ECMC algorithm will generally be more efficient when the solution varies greatly over a time step or when very low statistical noise is desired. Generally, the minimum number of histories per batch to obtain convergence with the LDFE trial space is larger than a piecewise constant representation because additional histories are needed to sufficiently estimate the first moment in x and μ of the intensity. Our formulation of the LO equations and consistency terms contrasts greatly from the typical formulation in Refs. 6, 7, and 8.

In this work, we demonstrate the utility of an S_2-like LO operator[11] in conjunction with an ECMC method[10] for the HO solver. The ECMC algorithm uses information about the intensity from the previous time step to reduce statistical noise to the same order as the HOLO iteration error with significantly less particle histories than SMC simulations, with less computational cost than IMC per history. We have derived the LO operator directly from the transport equation, using a LDFE spatial discretization for the HO and LO solutions. Herein we describe the algorithm and present results for 1-D gray test problems.

II. OVERVIEW OF THE HOLO ALGORITHM

For simplicity, our HOLO method will use a backward Euler discretization in time, as well as constant specific heats and cellwise-constant cross sections. The time-discretized equations are

$$\mu\frac{\partial I^{n+1}}{\partial x} + \left(\sigma_t^{n+1} + \frac{1}{c\Delta t}\right)I^{n+1} = \frac{\sigma_s}{2}\phi^{n+1} + \frac{1}{2}(\sigma_a acT^4)^{n+1} + \frac{I^n}{c\Delta t} \quad (3)$$

and

$$\rho c_v\frac{T^{n+1} - T^n}{\Delta t} = \sigma_a^{n+1}\phi^{n+1} - \sigma_a ac(T^4)^{n+1}, \quad (4)$$

where Δt is the uniform time-step size and the superscript n is used to indicate the n'th time step. Cross sections are evaluated at the end-of-time-step temperature, i.e., $\sigma_a^{n+1} \equiv \sigma_a(T^{n+1})$. In IMC, the time derivative in Eq. (1) is typically treated continuously using time-dependent MC over each time step. Our HO transport equation is discrete in time for simpler application of ECMC and to avoid difficulties in coupling to the fully discrete LO solver. However, this does introduce some artificial propagation of energy due to the implicit time differencing in optically thin regions.

In the HOLO context, the LO solver models isotropic scattering and resolves the material temperature spatial distribution $T(x)$ at each time step. The LO equations are formed via half-range angular and spatial moments of Eqs. (3) and (4), formed over a spatial FE mesh. The angular treatment in the LO equations has the same form as those used in the hybrid-S_2 method in Ref. 11, with element-averaged consistency parameters that are analogous to a variable Eddington factor. If the angular consistency parameters were exact, then the LO equations are exact, neglecting spatial discretization errors. These consistency parameters are lagged in each LO solve, estimated from the previous HO solution for $I^{n+1}(x,\mu)$, as explained below. For the initial LO solve for each time step, the parameters are calculated with $I^n(x,\mu)$. The discrete LO equations always conserve total energy, independent of the accuracy of the consistency terms. The LO system uses a LDFE spatial discretization for the temperature and half-range scalar intensities. The LDFE spatial discretization should correctly preserve the equilibrium diffusion limit, a critical aspect for TRT equations.[12,13] Additionally, the implicit time discretization with sufficient convergence of the nonlinear emission source will ensure that the method will not exhibit maximum principle violations.[14]

The solution to the LO system is used to construct a LDFE spatial representation of the isotropic scattering and emission sources on the right side of Eq. (3). The LDFE representation of the emission source mitigates the teleportation error. This defines a fixed-source pure-absorber transport problem for the HO operator. This HO transport problem represents a characteristic method that uses MC to invert the continuous streaming plus removal operator with an LDFE representation of sources; the representation of sources is similar to the linear moments method discussed in Ref. 15. We will solve this transport problem using ECMC. The output from ECMC is $\tilde{I}^{n+1}(x,\mu)$, a space-angle LDFE projection of the exact solution $I^{n+1}(x,\mu)$ to the described transport problem. Once computed, $\tilde{I}^{n+1}(x,\mu)$ is used to directly evaluate the necessary consistency parameters for the next LO solve. Since there is a global functional representation of the angular intensity, LO parameters are estimated using quadrature and do not require additional tallies. The HO solution is not used to directly estimate a new temperature at the end of the time step; it is only used to estimate the angular consistency

parameters for the LO equations, which eliminates typical operator splitting stability issues that require linearization of the emission source.

The process of performing subsequential HO and LO solves, within a single time step, can be repeated to obtain an increasingly accurate solution for $\phi^{n+1}(x)$ and $T^{n+1}(x)$. Thus, the HOLO algorithm, for the n'th time step, is as follows:

1. Perform a LO solve to produce an initial guess for $T^{n+1,0}(x)$ and $\phi^{n+1,0}(x)$, based on consistency terms estimated with $\tilde{I}^n$.

2. Solve the HO system for $\tilde{I}^{n+1,k+1/2}(x,\mu)$ with ECMC, based on the current LO estimate of the emission and scattering sources.

3. Compute LO consistency parameters with $\tilde{I}^{n+1,k+1/2}$.

4. Solve the LO system with HO consistency parameters to produce a new estimate of $\phi^{n+1,k+1}$ and $T^{n+1,k+1}$.

5. Optionally repeat 2 to 4 until the desired convergence is achieved.

6. Store $\tilde{I}^n \leftarrow \tilde{I}^{n+1}$, and move to the next time step.

Here, the superscript k denotes the outer HOLO iteration. The consistency terms force the HO and LO solutions for $\phi^{n+1}(x)$ to be consistent to the order of the current HOLO iteration error, as long as the LDFE spatial representation can accurately represent $\phi(x)$ and $T(x)$.

III. FORMING THE LO SYSTEM

To form the LO system of equations, spatial moments are taken over each spatial cell i, $x \in [x_{i-1/2}, x_{i+1/2}]$, weighted with the standard linear FE interpolatory basis functions. For example, the L moment operator is defined by

$$\langle\cdot\rangle_{L,i} = \frac{2}{h_i}\int_{x_{i-1/2}}^{x_{i+1/2}} b_{L,i}(x)(\cdot)dx \,, \tag{5}$$

where $h_i = x_{i+1/2} - x_{i-1/2}$ is the width of the spatial element and $b_{L,i}(x) = (x_{i+1/2} - x)/h_i$ is the FE basis function, for cell i, corresponding to position $x_{i-1/2}$. The right moment $\langle\cdot\rangle_{R,i}$ is defined with weight function $b_{R,i}(x) = (x - x_{i-1/2})/h_i$. In this notation, $\langle\phi\rangle_{L,i}$ and $\langle\phi\rangle_{R,i}$ represent spatial moments of the intensity over cell i, opposed to $\phi_{L,i}$ and $\phi_{R,i}$, which represent the interior value of the linear representation of $\phi(x)$ at $x_{i-1/2}$ and $x_{i+1/2}$ within the cell. To reduce the angular dimensionality, positive and negative half-range integrals of the angular intensity are taken. The half-range averages of I are defined as $\phi^+(x) = \int_0^1 I(x,\mu)d\mu$ and $\phi^-(x) = \int_{-1}^0 I(x,\mu)d\mu$. Thus, in terms of half-range quantities, $\phi(x) = \phi^-(x) + \phi^+(x)$.

III.A. Radiation Energy Equations

Pairwise application of the L and R basis moments with the $+$ and $-$ half-range integrals to Eq. (3) ultimately yields four moment equations per cell. As in Ref. 11, algebraic manipulation is performed to form intensity-weighted averages of μ, which we denote as consistency terms. As an example, the equation resulting from application of the L moment and positive half-range integral is

$$\begin{aligned} -2\,\mu_{i-1/2}^{n+1,+}\phi_{i-1/2}^{n+1,+} &+ \{\mu\}_{L,i}^{n+1,+}\langle\phi\rangle_{L,i}^{n+1,+} + \{\mu\}_{R,i}^{n+1,+}\langle\phi\rangle_{R,i}^{n+1,+} \\ &+ \left(\sigma_{t,i}^{n+1} + \frac{1}{c\Delta t}\right)h_i\langle\phi\rangle_{L,i}^{n+1,+} - \frac{\sigma_{s,i}h_i}{2}\left(\langle\phi\rangle_{L,i}^{n+1,+} + \langle\phi\rangle_{L,i}^{n+1,-}\right) \\ &= \frac{h_i}{2}\langle\sigma_a^{n+1}acT^{n+1,4}\rangle_{L,i} + \frac{h_i}{c\Delta t}\langle\phi\rangle_{L,i}^{n,+} \,, \end{aligned} \tag{6}$$

where the $\phi_{i-1/2}^+$ and $\mu_{i-1/2}^+$ terms represent face-averaged quantities at $x_{i-1/2}$. The negative direction and R moment equations are derived analogously. The element-averaged angular consistency terms are defined in terms of half-range integrals, e.g.,

$$\begin{aligned} \{\mu\}_{L,i}^{n+1,+} &\equiv \frac{\langle\mu I^{n+1}\rangle_{L,i}^+}{\langle I^{n+1}\rangle_{L,i}^+} \\ &= \frac{\frac{2}{h_i}\int_0^1\int_{x_{i-1/2}}^{x_{i+1/2}} \mu b_{L,i}(x)I^{n+1}(x,\mu)dxd\mu}{\frac{2}{h_i}\int_0^1\int_{x_{i-1/2}}^{x_{i+1/2}} b_{L,i}(x)I^{n+1}(x,\mu)dxd\mu} \,. \end{aligned} \tag{7}$$

The $\mu_{i-1/2}^{n+1,+}$ term is defined analogously and represents an angular average on the face at $x_{i-1/2}$.

III.B. Material Energy Equations

To derive the LO material energy equations, $T(x)$ is represented spatially in the LDFE trial space, i.e., $T(x) \simeq T_{L,i}b_{L,i}(x) + T_{R,i}b_{R,i}(x)$, $x \in (x_{i-1/2}, x_{i+1/2})$. Similarly, the emission term is represented in the material and radiation equations with the LDFE interpolant $T^4(x) \simeq T_{L,i}^4 b_{L,i}(x) + T_{R,i}^4 b_{R,i}(x)$. The L and R spatial moments are taken of the material energy equations; the LDFE representations for $T(x)$ and $\sigma_a acT^4(x)$ are used to simplify the spatial integrals. For example, the final LO material energy equation resulting from application of the L moment is

$$\frac{\rho_i c_{v,i}}{\Delta t}\left[\left(\frac{2}{3}T_{L,i}+\frac{1}{3}T_{R,i}\right)^{n+1}-\left(\frac{2}{3}T_{L,i}+\frac{1}{3}T_{R,i}\right)^{n}\right] + \sigma_{a,i}^{n+1}\left(\langle\phi\rangle_{L,i}^{+}+\langle\phi\rangle_{L,i}^{-}\right)^{n+1}=\sigma_{a,i}^{n+1}ac\left(\frac{2}{3}T_{L,i}^{4}+\frac{1}{3}T_{R,i}^{4}\right)^{n+1}. \quad (8)$$

Cross sections have been assumed constant over each element, evaluated at the average temperature within the element, i.e., $\sigma_{a,i}^{n+1}=\sigma_{a,i}([T_{L,i}^{n+1}+T_{R,i}^{n+1}]/2)$. Because the material energy balance contains only angularly integrated quantities, there is no need to take angular moments of the above equation.

III.C. Closing the System with Information from the HO Solution

The six degrees of freedom (DOFs) over each cell i are the four moments $\langle\phi\rangle_{L,i}^{+}$, $\langle\phi\rangle_{R,i}^{+}$, $\langle\phi\rangle_{L,i}^{-}$, and $\langle\phi\rangle_{R,i}^{-}$ and the two spatial edge values $T_{L,i}$ and $T_{R,i}$. The four radiation and two material energy equations define a system of equations for the six DOFs, coupled to other cells via upwinding in the streaming term. The relation between the volume and face-averaged quantities and the angular consistency parameters [e.g., Eq. (7)] are not known a priori. A lagged estimate of I^{n+1} from the previous HO solve is used to estimate the angular consistency parameters. In the HOLO algorithm, the equations for LO unknowns at iteration $k+1$ use consistency parameters computed [via relations, e.g., Eq. (7)] using the latest HO solution $\tilde{I}^{n+1,k+1/2}$ as an approximation for $I^{n+1}(x,\mu)$. To close the LO system spatially, a LD spatial closure with the usual upwinding approximation is used. For example, for positive flow [e.g., Eq. (6)], the face terms $\mu_{i-1/2}$ and $\phi_{i-1/2}$ are upwinded from the previous cell $i-1$ or from a boundary condition; the terms at $x_{i+1/2}$ are linearly extrapolated, computed using the L and R basis moments, e.g., $\phi_{i+1/2}^{+}=2\langle\phi\rangle_{R}^{+}-\langle\phi\rangle_{L}^{+}$. Because there are no derivatives of T in Eq. (4), there is no need to define T on the faces; the temperature has been assumed linear within a cell to relate T and T^4.

The choice of a LD spatial closure should preserve the equilibrium diffusion limit. In this limit, the MC HO solution will estimate angular consistency terms associated with an isotropic intensity, based on a spatially LD emission source. The isotropic-intensity consistency terms will produce LO equations that are equivalent to S_2 equations, with quadrature points of $\pm 1/2$. Because the spatial closure produces equations that are equivalent to an LDFE solution to these equations, we expect the equations to preserve the equilibrium diffusion limit.[13,16]

The LD closure with upwinding is not strictly positive. In particular, for optically thick cells with a steep intensity gradient, the solution becomes negative. These negative values of intensity can propagate to adjacent cells. In thick regions of TRT problems, reasonably fine spatial cells can still be of the order of millions of mean free paths (mfp); negative values with an LD representation are unavoidable in practice for such cells and mesh refinement is of minimal use. Typically, for a standard LDFE method, the equations are lumped to produce a strictly positive solution (for 1-D) (Ref. 13). However, standard FE lumping procedures would introduce difficulties in computing the consistency terms from the HO solution. Thus, an alternative spatial closure is used that is equivalent to the standard FE lumping procedure. The L and R moments are defined the same as before, preserving the average within a cell, but the relation between the moments and the outflow is modified. For example, for positive μ, the outflow is now defined as $\phi_{i+1/2}^{+}=\langle\phi\rangle_{R}^{+}$. Because the basis function $b_{R,i}(x)$ is strictly positive, the outflow is positive. This closure is used only in cells where negative intensities occur. For simplicity, we also use standard FE lumping for $T(x)$ and $T^4(x)$ in the material balance equations, e.g., Eq. (8).

III.D. Solving the Nonlinear LO System

We have used Newton's method to solve the global system of coupled LO equations, based on a typical linearization of the Planckian source with cross sections evaluated at temperatures of the previous iteration, as described in Ref. 13. Once the system is linearized, a discrete matrix equation is formed. Isotropic scattering, including effective scattering terms from the linearization, are included in the system matrix. The system matrix is an asymmetric, banded matrix with a band width of seven and is inverted directly. Newton iterations are repeated until $\phi^{n+1}(x)$ and $T^{n+1}(x)$ converge to a desired relative tolerance. Convergence is calculated using the spatial L_2 norm of the change in $\phi^{n+1}(x)$ and $T^{n+1}(x)$, relative to the norm of each solution. The lumping-equivalent discretization discussed above is used for cells where the solution for ϕ^{n+1} becomes negative. When negative values for $\phi^{n+1,\pm}(x)$ are detected, the lumping-equivalent discretization is used within those cells and that Newton step is repeated.

IV. THE ECMC HO SOLVER

The transport equation to be solved by the HO solver is

$$\mu\frac{\partial I^{n+1,k+1/2}}{\partial x}+\left(\sigma_t^k+\frac{1}{c\Delta t}\right)I^{n+1,k+1/2}=\frac{\sigma_s}{2}\phi^{n+1,k}+\frac{1}{2}(\sigma_a^k acT^4)^{n+1,k}+\frac{\tilde{I}^n}{c\Delta t}, \quad (9)$$

where the superscript k represents the outer HOLO iteration index. Material property indices will be suppressed from now on. Here, $k + 1/2$ denotes the ECMC solution within the outer HOLO iteration k, whereas k and $k + 1$ represent successive LO solves. The sources at k in Eq. (9) are estimated by the previous LO solution. Cross sections are evaluated at $T^{n+1,k}$. As all sources on the right side of the equation are known, this defines a fixed-source pure-absorber transport problem. We will solve this equation using ECMC. A more detailed description of the ECMC method can be found in Ref. 10, but a brief overview is given here. A general proof of exponential convergence for related adaptive MC transport methods with a different formulation is depicted in Ref. 17.

In operator notation, Eq. (9) can be written as

$$\mathbf{L}^k I^{n+1,k+1/2} = q^k \ , \tag{10}$$

where $I^{n+1,k+1/2}$ is the transport solution of the angular intensity based on the k'th LO estimate of q^k. The linear operator $\mathbf{L}^k$ is the continuous streaming plus removal operator defined by the left side of Eq. (3). The m'th approximate LDFE solution to Eq. (10) (m is the index of inner HO batches) is represented as $\tilde{I}^{n+1,(m)}$. The m'th residual is defined as $r^{(m)} = q - \mathbf{L}^k \tilde{I}^{n+1,(m)}$. For reference, the residual at iteration m in the HO solve is

$$r^{(m),k+1/2} = \frac{\sigma_s}{2}\phi^{n+1,k} + \frac{1}{2}(\sigma_a a c T^4)^{n+1,k} + \frac{\tilde{I}^n}{c\Delta t} - \left(\mu \frac{\partial \tilde{I}^{n+1,k+1/2}}{\partial x} + \left(\sigma_t + \frac{1}{c\Delta t}\right)\tilde{I}^{n+1,k+1/2}\right)^{(m)} , \tag{11}$$

where the k terms are LD in space on the coarsest mesh and are not recalculated at any point during the HO solve. The functional form of $\tilde{I}^n$ is defined from the final HO solution of the previous time step.

The addition of $\mathbf{L}I^{n+1} - q = 0$ to the residual equation and manipulation of the result yields the error equation

$$\mathbf{L}(I^{n+1} - \tilde{I}^{n+1,(m)}) = \mathbf{L}\epsilon^{(m)} = r^{(m)} \ , \tag{12}$$

where I^{n+1} is the exact solution and $\epsilon^{(m)}$ is the true error in $\tilde{I}^{n+1,(m)}$. We have suppressed the HOLO iteration indices because the LO estimated q^k and $\mathbf{L}^k$ remain constant over the entire HO solve. The $\mathbf{L}$ operator in the above equation is inverted, yielding the MC LDFE projection of the error in $\tilde{I}^{n+1,(m)}$, i.e.,

$$\tilde{\epsilon}^{(m)} = \mathbf{L}^{-1} r^{(m)}, \tag{13}$$

where $\mathbf{L}^{-1}$ is the MC inversion of the streaming and removal operator. This inversion is strictly a SMC simulation. The exact error in $\tilde{I}^{n+1,(m)}$ [with respect to Eq. (9)] is estimated with MC; tallies produce a projection of the error onto a LDFE space-angle trial space. The space-angle moments of the error computed as $\tilde{\epsilon}^{(m)}$ can be added to the moments of $\tilde{I}^{n+1}(m)$ to produce a more accurate solution.

Here, we emphasize the solution $\tilde{I}^{n+1,(m)}$ represents the LDFE projection of the exact MC solution to the transport problem defined by Eq. (9). The discretization error is in q, i.e., the LD spatial representation of the emission and scattering source and the LDFE space-angle projection $\tilde{I}^n(x,\mu)$. The projection of the intensity is, in general, far more accurate than a standard FE solution, e.g., a S_N collocation method in angle. In typical IMC calculations, the average energy deposition within a cell is computed using a standard path-length volumetric flux tally; the zeroth moment of the LDFE projection of ϵ is computed using an equivalent tally, preserving the zeroth moment of the error.

Volumetric flux tallies over each space-angle element are required to estimate $\tilde{\epsilon}^{(m)}$. The LD approximation in space is used to relate the outflow within a cell to the volumetric moments, eliminating the need for face-averaged tallies. The procedure for representing the solution, sampling with negative- and positive-weight particles, and tally definitions are given in Appendix A.

The ECMC algorithm is as follows:

1. Initialize the guess for $\tilde{I}^{n+1,(0)}$ to $\tilde{I}^n$ or the projection of $\tilde{I}^{n+1}$ from the latest HO solve.

2. Compute $r^{(m)}$.

3. Perform a MC simulation to obtain $\tilde{\epsilon}^{(m)} = \mathbf{L}^{-1} r^{(m)}$.

4. Compute a new estimate of the intensity: $\tilde{I}^{n+1,(m+1)} = \tilde{I}^{n+1,(m)} + \tilde{\epsilon}^{(m)}$.

5. Repeat steps 2 through 4 until the desired convergence criteria are achieved.

The initial guess for the angular intensity $I^{n+1,(0)}$ is computed based on the previous solution for $\tilde{I}^n$. This is a critical step in the algorithm; it significantly reduces the required number of particles per time step because the intensity does not change drastically between time steps in optically thick regions. The ECMC batch (steps 1 to 4 of the algorithm) results in essentially the same estimate of the solution as the residual formulation used in Ref. 8. The primary difference is that our method uses an LDFE trial space and iterates on the solution estimate by recomputing the residual.

Exponential convergence is obtained if the error ε is reduced in each batch. With each batch, a better estimate of the solution is used to compute the new residual,

decreasing the magnitude of the MC residual source at each iteration m, relative to the solution I^{n+1}. Each MC estimate of the moments of ϵ still has a statistical uncertainty that is governed by the standard $1/\sqrt{N}$ convergence rate,[18] for a particular source $r^{(m)}$, where N is the number of histories performed. If the statistical estimate of the projection $\tilde{\epsilon}$ is not sufficiently accurate, then the iterations would diverge. There is a statistical correlation across batches because $I^{n+1,(m+1)}$ and $\epsilon^{(m)}$ are correlated through $I^{n+1,(m)}$ and the MC source $r^{(m)}$.

Because the exact angular intensity does not, in general, lie within the LDFE trial space, the iterative estimate of the error will eventually stagnate once the error cannot be sufficiently represented by a given FE mesh. An adaptive h-refinement algorithm has been implemented that can be used to allow the system to continue converging toward the exact solution.[9,10] For TRT problems where absorption-reemission physics dominate, the diffusive and slowly varying regions of the problem require a less refined angular mesh to capture the solution than typical neutronics problems. However, greater spatial resolution is needed due to the steep spatial gradients. Once error stagnation has occurred (and mesh refinement has reached a maximum level), additional histories can be performed with a fixed residual source to estimate the remaining error in the current solution. Although the remaining error will converge statistically at a standard $1/\sqrt{N}$ convergence rate, it will be much smaller than for a SMC simulation, producing a much more efficient solution method overall.

For the HO solver, in cells near the radiation wave front, the LDFE trial space results in negative values of $\tilde{I}^{n+1}(x,\mu)$, similar to the LO solver. Because the residual formulation in ECMC allows for negative-weight particles to occur, currently we do not treat these cells specially. We detect if the consistency terms lie in the appropriate half-space at the end of the HO solve, an indication that the intensity was negative within that cell. If the terms are nonphysical, then they are replaced with the corresponding S_2-equivalent value. In general, in such cells where the trial space cannot accurately represent the solution, error stagnation will rapidly occur.

IV.A. Variance Reduction and Source Sampling

As in Ref. 7, because we are solving a pure-absorber problem with MC, we will allow particles to stream without absorption to reduce the statistical variance in the tallies. The weight of particles is reduced deterministically along the path as they stream, with no need to sample a path length. Because particles are exponentially attenuated, the normalized weight is adjusted as $w(x,\mu) = w(x_0,\mu)\exp(-\sigma_t|(x-x_0)/\mu|)$, where x_0 is the starting location of the path. The tallies account for the continuously changing weight, as given in Appendix A. Histories are allowed to stream in this manner for 6 mfp before switching to analog path length sampling; this limits the tracking of very small weight histories. The choice of 6 mfp allows particles to continuously deposit weight until they reach 0.25% of their original weight. Path lengths are tracked in terms of mfp, so there is no need to resample at material interfaces.

As another way to improve efficiency, a modified systematic sampling method[18] was used for determining source particle locations. The goal is to effectively distribute particle histories to regions of importance, but to sample a sufficient number of histories in less probable regions to prevent large statistical noise. However, there is no need to sample histories in regions in thermal equilibrium. The residual gives a good indication of where histories are most likely to contribute to the error, particularly in optically thick cells where particles do not transport over long distances. In the sampling algorithm, the number of particle histories sampled in each space-angle cell is predetermined and proportional to the magnitude of the residual, including face and volumetric sources, within that cell. Then, for the predetermined number of histories within a cell, the source location is randomly sampled according to the residual source distribution of that cell. In cells where the relative magnitude of the residual is of the order of the roundoff, no particle histories are sampled. In these regions, the problem remains in equilibrium and the solution is known exactly. For cells that are significant but have a predetermined number of histories below some preset minimum N_{min}, the number of histories sampled in that cell is set to N_{min}. This is to limit bad statistics in low probability cells (this would be important for adaptively refined meshes). In the simulations performed for this work, $N_{min} = 1$. This choice was made to keep the total number of histories per time step constant throughout the simulation for comparison to IMC.

V. COMPUTATIONAL RESULTS

We will compare results of the HOLO method to IMC with a source-tilting algorithm for two test problems.[19] Also, we briefly compare performance in Sec. V.C. For all IMC results, no local, discrete diffusion acceleration methods for effective scattering (e.g., those in Refs. 2 and 3) are applied. Finally, we will demonstrate the efficiency advantage of ECMC in our HOLO algorithm by comparing the results to the same HOLO algorithm if the ECMC algorithm is replaced with a SMC simulation. Results are

also given for a single ECMC batch, which is similar to a RMC method.

A measure of variance in cell-averaged scalar intensities was calculated to provide a quantitative measure of the statistical accuracy of different solution methods. To form sample standard deviations, 20 independent simulations for each particular result were performed using unique random number generator seeds. The variance of a particular cell-averaged $\phi(x)$ is

$$S_i^2 = \frac{20}{20-1}\sum_{l=1}^{20}(\overline{\phi_i} - \phi_i^l)^2 , \tag{14}$$

where ϕ_i^l is the cell-averaged scalar intensity for cell i from the l'th of 20 independent simulations and $\overline{\phi_i}$ is the corresponding sample mean from the 20 simulations. To provide a normalized, spatially integrated result, we form a norm over cells as

$$\|s\| = \left(\frac{\sum_{i=1}^{N_c} S_i^2}{\sum_{i=1}^{N_c} \overline{\phi_i}^2} \right)^{1/2} , \tag{15}$$

where N_c is the number of spatial cells.

We will also form a figure of merit (FOM) to demonstrate how statistical accuracy scales with the number of histories performed. Our FOM is defined as

$$\text{FOM} = \frac{1}{N_{tot}\|s\|^2} , \tag{16}$$

where N_{tot} is the total number of histories performed over the simulation. A larger value of the FOM indicates that the method produced less variance in the solution per history performed, for a given problem. This form of the FOM is typically chosen because the variance is expected to reduce inversely proportional to N_{tot}, so for SMC simulations the FOM becomes, on average, independent of N_{tot} (Ref. 18). The FOM is not necessarily expected to be independent of N_{tot} for IMC or our HOLO method due to the correlation of the solution between time steps; additionally, ECMC has correlations between batches.

V.A. Marshak Wave

For the first problem, the radiation and material energies are initially in equilibrium at 2.5×10^{-5} keV. An isotropic incident intensity of 0.150 keV is applied at $x = 0$; the incident intensity on the right boundary is 2.5×10^{-5} keV. The material properties are $\rho = 1\ \text{g} \cdot \text{cm}^{-3}$ and $c_v = 0.013784$ jks/(keV · g). The absorption cross section varies as $\sigma(T) = 0.001\ \rho\ T^{-3}$ (cm^{-1}). The simulation was advanced until $t = 5$ sh (1 sh $\equiv 10^{-8}$ s) with a fixed time-step size of 0.001 sh. For comparison, we have not used AMR, performed only one HOLO iteration per time step, and used a fixed three HO batches with an equal number of histories per batch. A relative tolerance of 10^{-6} for the change in $\phi(x)$ and $T(x)$ was used for the LO Newton solver for all results. Radiation energy distributions are plotted as an equivalent temperature given by $T_r = (\phi/(ac))^{0.25}$. Cell-averaged quantities are plotted. Although isotropic scattering is handled by the LO solver in the algorithm described above, we have considered only problems with $\sigma_s = 0$ here. Results for neutronics with isotropic scattering included are given in Ref. 9.

Figure 1a compares the cell-averaged radiation temperatures for the IMC and HOLO methods with ECMC, for various numbers of spatial mesh cells N_c; we have used HOLO-ECMC to denote our algorithm because later results will use different HO solvers. For all IMC calculations, $n = 10^5$ histories per time step were used. For the HOLO method, we have used four equal-sized cells in μ for the FE angular mesh used by the ECMC solver. The spatial grid is the same for the HO and LO solvers. For $N_c = 25$ and $N_c = 200$, 4000 histories per batch ($n =$ 12 000 per time step) were used. For $N_c = 500$, 16 000 histories per time step were used due to the increased number of space-angle cells that need to be sampled. The IMC and HOLO solutions agree as the mesh converges. There is similar agreement in the location of the wave front due to the linear shape of the emission source over a cell. The cells nearest the wave front required lumping-equivalent discretization and S_2-equivalent terms during the LO solve, resulting in strictly positive solutions.

Figure 1b compares solutions for 200 cells. For the IMC solution, 10^5 histories per time step were simulated; for the HOLO method, only 4000 histories per batch (12 000 per time step) were simulated. There is significant statistical noise in the IMC solution compared to the HOLO solution. The HOLO solution visually demonstrates no statistical noise. Because the ECMC solve is only determining the change over the time step, the statistical noise in the result is small relative to the magnitude of I^{n+1}. Also, the source sampling only places particles in cells where the residual is large. No particles are sampled in the equilibrium region in front of the wave.

Table I compares $\|s\|$ and the FOM for IMC and the HOLO methods, for different numbers of histories per time step. The FOM results are normalized to the value for IMC with $n = 12\,000$. The HOLO method demonstrates less variance for the same numbers of histories, producing FOM values that are two orders of magnitude greater than

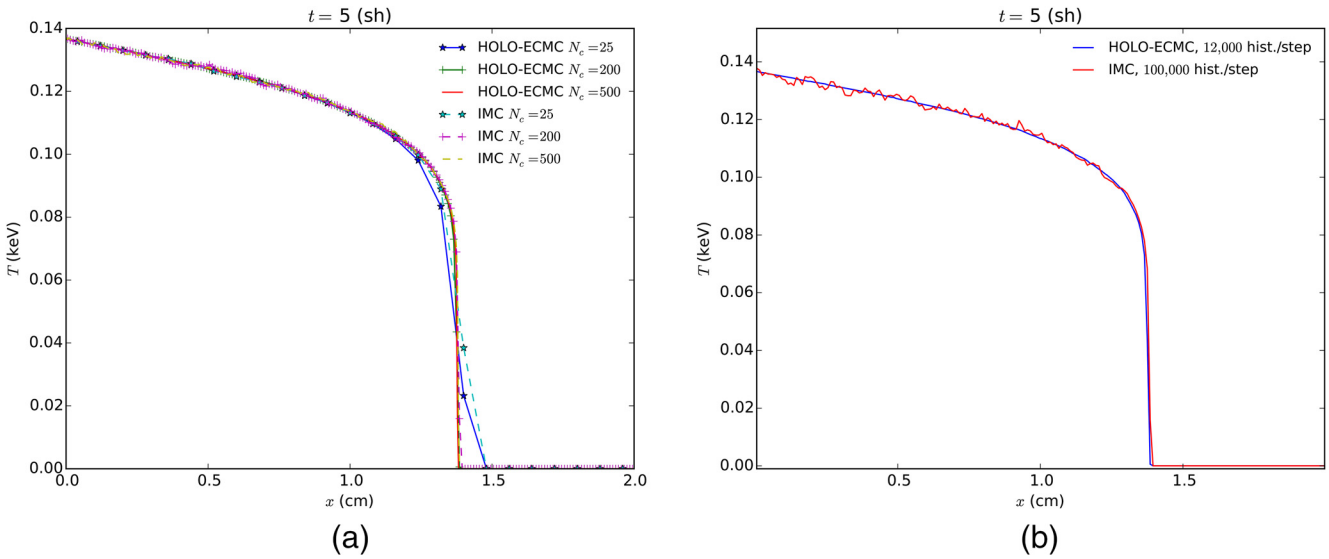

Fig. 1. Comparison of radiation temperatures for Marshak wave problem at $t = 5$ sh. (a) Convergence of IMC and HOLO-ECMC solutions. (b) Comparison of solutions for 200 spatial cells.

TABLE I

Comparison of Sample Statistics for the Marshak Wave Problem*

	$\|\|s\|\|$		FOM	
Histories per Time Step	IMC	HOLO-ECMC	IMC	HOLO-ECMC
12 000	3.40%	0.28%	1	145
100 000	1.22%	0.057%	0.93	422

*Simulation end time is $t = 5$ sh.

TABLE II

Material Properties for Two-Material Problem

	$x \in [0, 0.5)$ cm	$x \in [0.5, 1.0]$ cm
σ_a (cm^{-1})	0.2	2000
ρ (g · cm^{-3})	0.01	10.0
c_v [jks/(keV · g)]	0.1	0.1

for IMC. Whereas the FOM remains relatively constant for IMC, as n is increased the FOM improves for the HOLO method. This is a result of each batch producing more statistically accurate estimates of the error ϵ, which results in an increased convergence rate of ϵ overall.

V.B. Two-Material Problem

This problem consists of an optically thin (left) and an optically thick (right) material region, with temperature-independent cross sections. The material properties are given in Table II. Initially, the radiation and material energies are in equilibrium at a temperature of 0.05 keV. An isotropic incident intensity of 0.500 keV is applied at $x = 0$ at $t = 0$; the isotropic incident intensity on the right boundary is 0.05 keV. The simulation end time is 5 sh. For all HOLO simulations, we have used eight equal-sized mesh cells in μ. As for the Marshak problem, the cells nearest the wave front required lumping-equivalent discretization and S_2-equivalent terms during the LO solve. Figure 2a compares the HOLO and IMC radiation temperatures at the end of the simulation. The IMC and HOLO results show good agreement over the finer mesh. On the coarse mesh ($N_c = 20$), the LDFE representation of T^4 in the HOLO method predicts the location of the wave front more accurately than the IMC method with source tilting.

Figure 2b demonstrates the benefit of ECMC as a HO solver compared to SMC. The HOLO algorithm with the ECMC HO solver (HOLO-ECMC) results are for running three batches of 10 000 histories per time step. The solution for the HOLO method with a SMC solver as the HO solver (HOLO-SMC) with standard source sampling uses 10^5 histories per time step. The HOLO-SMC solution demonstrates significant statistical noise. This noise is introduced into the LO solver by bad statistics in computing the consistency terms. Also plotted is an S_2 solution obtained with consistency terms that are equivalent to S_2 and no HO correction. The S_2 solution results in an artificially fast wave front, as expected, demonstrating the necessity of HO correction in this problem.

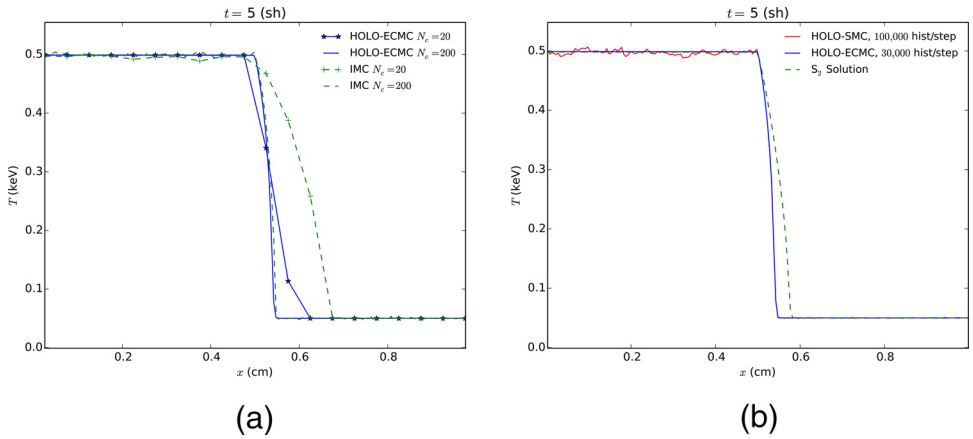

Fig. 2. Comparison of radiation temperatures for two-material problem. (a) Comparison of IMC and HOLO-ECMC. (b) Comparison of SMC and ECMC HO solvers.

Table III compares the FOM and $\|s\|$ for IMC and the HOLO-ECMC method. The FOM values are normalized to the value for IMC with $n = 30\,000$. The end time was reduced to 2 sh for these results to reduce computational times. The reduction in variance by the HOLO method over IMC is substantial. The improvement of the FOM for the HOLO method compared to IMC is greater than for the Marshak wave problem. This improvement is because the wave moves much slower in the right region of this problem, due to the large constant cross section. Also, in the optically thin region of the problem, the solution quickly comes to equilibrium. Thus, the ECMC algorithm has to estimate a very small change in the intensity over a time step. Additionally, difficulties in resolving the solution at the wave front are not as severe compared to the Marshak wave problem, where the cold cells have a much larger cross section.

TABLE III

Comparison of Sample Statistics for the Two-Material Problem for 200 x Cells*

	$\|s\|$		s_{max}	
Histories per Time Step	IMC	HOLO-ECMC	IMC	HOLO-ECMC
30 000	3.63%	0.01%	1	104 000
100 000	1.96%	0.003%	1.03	360 000

*Simulation end time is $t = 2$ sh.

V.C. Performance Comparison of IMC and HOLO-ECMC

We have measured the total CPU time for simulations to provide a simplified measure of the computational cost. These results compare how computational times change the two different problems and how the methods scale with time-step size and particle histories. Absolute comparisons in the computational cost of the two methods cannot be made because the methods are implemented in different code infrastructures. Additionally, the HOLO method fully resolves nonlinearities at each time step, whereas IMC uses a single linearized step with lagged cross sections. Simulations were performed on the same processor, using a single CPU core. Reported times are the average of ten runs and all results used 200 x cells, $\Delta t = 0.001$ sh, and an end time of $t = 2$ sh.

Table IV compares the average simulation time per history performed for the Marshak wave problem. The average time per history is computed by dividing the total simulation time by the total number of histories performed (e.g., the time of the LO solves is included for the HOLO method).

TABLE IV

Comparison of Average CPU Times per History and LO Iteration Counts for the Marshak Wave Problem

Histories per Time Step	Δt (sh)	IMC (μs/history)	HOLO-ECMC (μs/history)	Newton Iterations per LO Solve
100 000	0.001	10	5.3	3.8
12 000	0.001	9.7	8.1	4.1
12 000	0.005	19	9.4	6.2

Results are given for different numbers of histories per time step, as well as with an increased time-step size. Table IV also includes the number of LO iterations performed per LO solve for the HOLO method, averaged over all time steps; there are two LO solves per time step. The same results are reported for the two-material problem in Table V.

The HOLO method does not scale with the number of histories due to the fixed cost of the LO solver. The cost of the LO solver is more significant at the lower history counts compared to the case of 10^5 histories, for both problems. There is a slight increase in the number of Newton iterations as the time step is increased, but the average cost per history is not significantly increased. Like the results in Ref. 7, as the time-step size is increased to 0.005 sh, the IMC method increases in cost per time step, due to an increase in effective scattering events, particularly for the two-material problem. Because the cross sections in the two-material problem do not have a T^{-3} behavior, the cost of the effective scattering cross section in IMC is more apparent, resulting in longer simulation times.

V.D. Comparison of Different HO Solvers

In this section, we compare the results of our HOLO algorithm with different HO solvers for the test problems in Secs. V.A. and V.B. We compare SMC as a HO solver to the HOLO algorithm with ECMC using both three batches and a single batch, per time step. The use of a single batch is similar to the approach in Ref. 8. Results are tabulated for 200 x cells, using the same total number of histories per time step, divided evenly among the batches.

Tables VI and VII compare the results for the Marshak wave and two-material problems. The number of batches for each ECMC case is indicated in parentheses. The FOM values are normalized to the reference IMC result for the corresponding problem. For HOLO-SMC, there is minimal reduction in variance compared to IMC in the Marshak wave problem, and the two-material problem actually demonstrates worse variance. Sufficient histories are not performed to accurately estimate

TABLE V

Average CPU Times per History and LO Iteration Counts Required for the Two-Material Problem

Histories per Time Step	Δt (sh)	IMC (μs/history)	HOLO-ECMC (μs/history)	Newton Iterations per LO Solve
100 000	0.001	17	3.5	4.9
30 000	0.001	18	6.9	5.0
30 000	0.005	59	7.4	7.6

TABLE VI

Comparison of Sample Statistics for the Marshak Wave Problem*

	$\|\|s\|\|$			FOM		
Histories per Time Step	SMC	ECMC (1)	ECMC (3)	SMC	ECMC (1)	ECMC (3)
12 000	2.77%	0.10%	0.28%	1.50	1280	145
100 000	0.98%	0.03%	0.06%	1.43	1270	422

*Number of ECMC batches is indicated in parentheses.

TABLE VII

Comparison of Sample Standard Deviations for the Two-Material Problem*

	$\|\|s\|\|$			FOM		
Histories per Time Step	SMC	ECMC (1)	ECMC (3)	SMC	ECMC (1)	ECMC (3)
30 000	5.35%	0.002953%	0.011%	0.46	1.51×10^6	1.04×10^4
100 000	2.85%	0.001474%	0.0033%	0.49	1.80×10^6	3.59×10^4

*Number of ECMC batches is indicated in parentheses.

consistency terms throughout the problem. For ECMC, a single batch produces less variance than three equal batches. This indicates that if the solution cannot be resolved with the trial space (i.e., the intensity is driven negative), a single large batch may be more accurate. These results account only for statistical variance, and do not account for accuracy, which will depend on the estimates of ϵ computed each iteration.

V.E. Preheated Marshak Wave Problem and AMR

Finally, to demonstrate the potential of ECMC with adaptive space-angle mesh refinement, we performed a modified Marshak wave problem. The problem is modified so that the LDFE trial space can accurately represent the solution (i.e., the intensity is strictly positive). Mesh refinement is of minimal use in the previous problems due to most of the error existing at the wave fronts, caused by the large cross sections. The modified problem has the same material properties and left boundary source as the Marshak wave problem in Sec. V.A. However, the initial equilibrium temperature and right boundary condition are raised to 0.03 keV. The higher initial temperature reduces the initial cross section and increases the strength of the emission source within cells. The LDFE mesh can now sufficiently resolve the solution and lumping is not required by the LO solution. The simulation end time is 0.5 sh with a constant time step of $\Delta t = 0.001$ sh.

Figure 3 compares the result from HOLO-ECMC with three batches and IMC. It was found that 100 x cells were sufficient to resolve the solution spatially. There is slightly more noise in IMC past the wave front due to the increased emission source. Additionally, the opacity is thin enough that some photon energy is able to reach the right boundary, in front of the wave front.

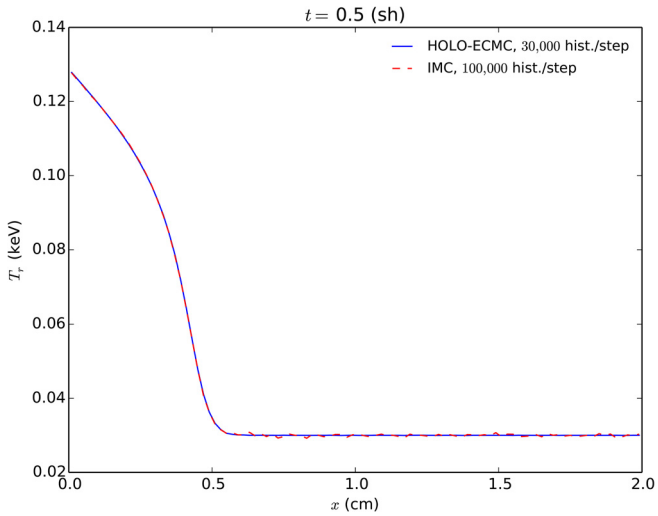

Fig. 3. Comparison of radiation temperatures for the preheated Marshak wave problem for 100 x cells at $t = 0.5$ sh.

Table VIII compares the variances for this problem for the various HO solvers. The FOM values are normalized to HOLO-SMC with 12 000 histories per time step. The final row of Table VIII is for an ECMC simulation with AMR. The strategy for refinement is described in Appendix B. The AMR case used a total of nine batches, with a refinement occurring at the end of the third and sixth batches, for every time step. The initial number of histories was adjusted so that the average number of histories per time step is near 100 000; on average 99 881 histories per time step were used. All ECMC meshes used four equally spaced μ cells initially. The improvement in variance by ECMC compared to SMC is not as significant as for the other problems. This is a result of the reduced opacity leading to the intensity changing throughout the spatial and angular domains. The FOM is highest for ECMC with adaptive refinement. When the solution can be resolved, the adaptive algorithm allows for a higher convergence rate of statistical variance. The consistency terms and LO solution are still computed over the fixed coarser mesh. However, in general, the refined mesh can produce higher accuracy in consistency terms that is not being measured by the FOM.

VI. CONCLUSIONS

We have been able to produce solutions for Marshak wave test problems using a new HOLO method that are in agreement with IMC. Unlike IMC, our method requires no effective scattering events to be included in the MC simulation, which limits the run time of particle tracking, while adding the cost of a LO Newton solver. Average LO iteration counts did not significantly increase as the time-step size was increased. The LDFE spatial representation mitigates issues with teleportation error, producing results with spatial accuracy comparable to IMC with source tilting. The ECMC approach, with initial guesses based on the previous radiation intensity, results in an efficient reduction of statistical error and allows for particles to be distributed to largely varying regions of the problem. The LO solver resolves the nonlinearities in the equations, resulting in a fully implicit time discretization. The LO solver can accurately and efficiently resolve the solution in diffusive regions, while the HO transport solver provides the accuracy of a full transport treatment where necessary.

The primary difficulty to overcome in the ECMC algorithm is when the solution cannot be accurately

TABLE VIII

Comparison of Sample Statistics for the Preheated Marshak Wave Problem for 100 x Cells*

	$\|s\|$			FOM		
Histories per Time Step	SMC	ECMC (1)	ECMC (3)	SMC	ECMC (1)	ECMC (3)
12 000	0.86%	0.13%	0.24%	1	41	13
100 000	0.16%	0.042%	0.08%	3.32	52	15
99 881 (AMR, nine batches)	—	0.038%		—	61	

*Number of ECMC batches is indicated in parentheses.

represented by the trial space, e.g., in optically thick cells where the solution is driven negative. We are currently developing an approach to allow the ECMC iterations to continue converging globally when there are such regions. It is necessary to ensure the closure in the LO system is consistent with the HO representation for the solution in such regions. The ability to represent the solution accurately in rapidly varying regions of the problem will be key for generalization of this method to higher dimensions. A formulization of the ECMC method that allows for time-continuous MC transport (similar to IMC) is also currently being investigated. This may reduce some of the loss of accuracy in optically thin regions due to the time discretization of the transport equation in the HO solver. However, greater time accuracy is not of primary concern as this method is intended for use in problems dominated by large absorption opacities, where the LO acceleration is critical. Inclusion of Compton scattering in this algorithm, which would introduce additional nonlinear dependence through energy exchange with the material, is a topic for future research.

Future work will also explore the accuracy of the HOLO method, in particular, analyzing the optimal number of batches and the benefit of adaptive refinement. This will likely require manufactured solutions. The sensitivity of the method to mesh sizes and time-step sizes will be investigated more thoroughly. Ultimately, we plan to extend this method to multiple spatial dimensions for the multigroup TRT equations. For TRT problems, it is important that the LO spatial discretization satisfies the equilibrium diffusion limit. To extend to higher dimensions, our LDFE representation may require a higher-degree spatial representation for the LO system to achieve the diffusion limit. Further asymptotic analysis of the method will be applied before implementation. It may be necessary to use a different LO system (e.g., the nonlinear diffusion acceleration approach in Ref. 8), if the S_2-like equations become too inefficient or difficult to implement in higher dimensions. Alternatively, a variable Eddington tensor approach may provide more stability in rapidly variable regions of the problem while still allowing for a consistent LDFE solution that is efficiently solvable.

APPENDIX A

IMPLEMENTATION OF ECMC FE SPACE, TALLIES, AND RESIDUAL SAMPLING

The ECMC solver uses a FE representation in space and angle. On the interior of the cell with the i'th spatial index and j'th angular index, the linear representation is defined as

$$\tilde{I}(x,\mu) = I_{a,ij} + \frac{2}{h_x} I_{x,ij}(x - x_i) + \frac{2}{h_\mu} I_{\mu,ij}(\mu - \mu_j) \ ,$$

$$x_{i-1/2} < x < x_{i+1/2} \ , \quad \mu_{j-1/2} \le \mu \le \mu_{j+1/2} \ .$$

The spatial cell width is h_x, the angular width is h_μ, the center of the cell is (x_i,μ_j), and

$$I_{a,ij} = \frac{1}{h_x h_\mu} \iint_{\mathcal{D}} I(x,\mu) dx d\mu \ , \tag{A.1}$$

$$I_{x,ij} = \frac{6}{h_x h_\mu} \iint_{\mathcal{D}} \left(\frac{x - x_i}{h_x} \right) I(x,\mu) dx d\mu \ , \tag{A.2}$$

and

$$I_{\mu,ij} = \frac{6}{h_x h_\mu} \iint_{\mathcal{D}} \left(\frac{\mu - \mu_j}{h_\mu} \right) I(x,\mu) dx d\mu \ , \tag{A.3}$$

where $\mathcal{D} : x_{i-1/2} \le x \le x_{i+1/2} \times \mu_{j-1/2} \le \mu \le \mu_{j+1/2}$. Standard upwinding in space is used to define $I(\mu)$ on incoming faces.

This representation can directly be plugged into Eq. (11) and evaluated to produce the residual source in the ECMC HO transport problem. The MC source $r^{(m)}(x,\mu)$ in Eq. (13) consists of both face and volumetric

sources and can produce positive- and negative-weight particles. The distribution for sampling particle coordinates, in space and angle, is based on the L_1 norm over space and angle of the residual.[10] A particular cell volume or face is sampled, and then rejection sampling[18] is used to sample from the appropriate distribution on the face or interior of the space-angle cell. If the residual is negative at the sampled coordinates, the weight of the particle history is negative.

During a MC batch, moments of the error are tallied. The necessary moments of the error are defined analogously to Eqs. (A.1), (A.2), and (A.3). The tallies are evaluated by weighting the particle density with the appropriate basis function and integrating along the history path through the cell. For the cell average, the n'th particle makes the contribution

$$\epsilon^n_{a,ij} = \frac{1}{h_x h_\mu} \int_{s^n_o}^{s^n_f} w^n(x,\mu) ds \,, \tag{A.4}$$

where s^n_o and s^n_f are the beginning and end of the n'th particle track in the cell and $w(x,\mu)$ is the weight of the error particle in the MC simulation. The weight is attenuated exponentially, i.e., $w(x,\mu) \propto \exp(-\sigma_t|x/\mu|)$. Substitution of the exponential attenuation of the weight produces the result

$$\epsilon^n_{a,ij} = \frac{w(x_0,\mu)}{\sigma_t h_x h_\mu}\left(1 - e^{-\sigma_t s^n}\right). \tag{A.5}$$

Here, $w(x_0,\mu)$ is the particle weight at the start of the path and s^n is the length of the track. The contribution of a particle track to ϵ_x is given by

$$\epsilon^n_{x,ij} = \frac{w(x_0,\mu)}{h_x^2 h_\mu \sigma_t}\left[x_0 - x_f e^{-\sigma_t s^n} + \left(\frac{\mu}{\sigma_t} - x_i\right)\left(1 - e^{-\sigma_t s^n}\right)\right], \tag{A.6}$$

where x_0 and x_f are the beginning and ending x coordinates of the n'th path. The contribution to the first moment in μ is

$$\epsilon^n_{\mu,ij} = \frac{w(x_0,\mu)}{h_\mu^2 h_x \sigma_t}(\mu - \mu_j)\left(1 - e^{-\sigma_t s^n}\right), \tag{A.7}$$

where the particle x-direction cosine μ does not change because it is a pure-absorber simulation. Finally, the moments of the error are simply the average contribution of all particles.

APPENDIX B

ADAPTIVE MESH REFINEMENT

This section describes the adaptive refinement strategy for the ECMC algorithm. Detailed equations for performing projections between meshes and computing the residual source on the refined meshes can be found in Ref. 10. At the end of the ECMC batch, refinement is performed in space-angle cells based on a jump indicator, which is the magnitude of the difference between $I(x,\mu)$ in adjacent cells, averaged over each edge. The value of the largest jump, out of the four edges within a cell, is used as the indicator for that cell. Based on this indicator, the 20% of cells with the largest jump are refined. Future work will explore simply using ϵ to indicate refinement, rather than the jump error. The refinement of a cell is chosen to be symmetric, with each space-angle cell divided into four equal-sized cells. The solution for $\tilde{I}^{n+1}(x,\mu)$ of the batch is projected onto the finer mesh for the next batch. Because the dimensionality of the sample space has increased, we increase the number of histories per batch such that the ratio of the number of histories to total cells is approximately constant for all meshes. At the end of the last HO solve in a time step, $\tilde{I}^{n+1}$ is projected back onto the original coarsest mesh and stored as $\tilde{I}^n$ for the next time step.

Acknowledgments

This research was supported with funding received from the U.S. Department of Energy (DOE) Office of Nuclear Energy's Nuclear Energy University Programs, the DOE National Nuclear Security Administration, under award DE-NA0002376, and under Los Alamos National Security, LLC, for the National Nuclear Security Administration of the DOE under contract DE-AC52-06NA25396.

References

1. J. A. FLECK JR. and J. D. CUMMINGS JR., "An Implicit Monte Carlo Scheme for Calculating Time and Frequency Dependent Nonlinear Radiation Transport," *J. Comput. Phys.*, **8**, *3*, 313 (1971); http://dx.doi.org/10.1016/0021-9991(71)90015-5.
2. N. GENTILE, "Implicit Monte Carlo Diffusion: An Acceleration Method for Monte Carlo Time-Dependent Radiative Transfer Simulations," *J. Comput. Phys.*, **172**, *2*, 543 (2001); http://dx.doi.org/10.1006/jcph.2001.6836.
3. J. D. DENSMORE, K. G. THOMPSON, and T. J. URBATSCH, "A Hybrid Transport-Diffusion Monte Carlo Method for Frequency-Dependent Radiative-Transfer Simulations," *J. Comput. Phys.*, **231**, *20*, 6924 (2012); http://dx.doi.org/10.1016/j.jcp.2012.06.020.

4. A. B. WOLLABER, E. W. LARSEN, and J. D. DENSMORE, "A Discrete Maximum Principle for the Implicit Monte Carlo Equations," *Nucl. Sci. Eng.*, **173**, *3*, 259 (2013); http://dx.doi.org/10.13182/NSE11-101.

5. M. S. McKINLEY, E. D. BROOKS III, and A. SZOKE, "Comparison of Implicit and Symbolic Implicit Monte Carlo Line Transport with Frequency Weight Vector Extension," *J. Comput. Phys.*, **189**, *1*, 330 (2003); http://dx.doi.org/10.1016/S0021-9991(03)00213-4.

6. J. WILLERT et al., "A Hybrid Approach to the Neutron Transport *k*-Eigenvalue Problem Using NDA-Based Algorithms," *Proc. M&C 2013*, Sun Valley, Idaho, May 5–9, 2013, American Nuclear Society (2013).

7. H. PARK et al., "Monte Carlo Solution Methods in a Moment-Based Scale-Bridging Algorithm for Thermal Radiative Transfer Problems," *Proc. M&C 2013*, Sun Valley, Idaho, May 5–9, 2013, American Nuclear Society (2013).

8. J. WILLERT and H. PARK, "Residual Monte Carlo High-Order Solver for Moment-Based Accelerated Thermal Radiative Transfer Equations," *J. Comput. Phys.*, **276**, 405 (2014); http://dx.doi.org/10.1016/j.jcp.2014.07.039.

9. S. BOLDING and J. MOREL, "A High-Order Low-Order Algorithm with Exponentially-Convergent Monte Carlo for *k*-Eigenvalue Problems," *Trans. Am. Nucl. Soc.*, **111**, 637 (2014).

10. J. PETERSON, "Exponentially Convergent Monte Carlo for the 1-D Transport Equation," MS Thesis, Texas A&M University (2014).

11. E. WOLTERS, "Hybrid Monte Carlo—Deterministic Neutron Transport Methods Using Nonlinear Functionals," PhD Dissertation, University of Michigan (2011).

12. E. LARSEN, G. POMRANING, and V. BADHAM, "Asymptotic Analysis of Radiative Transfer Problems," *J. Quant. Spectrosc. Radiat. Transfer*, **29**, *4*, 285 (1983); http://dx.doi.org/10.1016/0022-4073(83)90048-1.

13. J. MOREL, T. WAREING, and K. SMITH, "Linear-Discontinuous Spatial Differencing Scheme for S_n Radiative Transfer Calculations," *J. Comput. Phys.*, **128**, 445 (1996); http://dx.doi.org/10.1006/jcph.1996.0223.

14. E. W. LARSEN, A. KUMAR, and J. E. MOREL, "Properties of the Implicitly Time-Differenced Equations of Thermal Radiation Transport," *J. Comput. Phys.*, **238**, 82 (Apr. 2013); http://dx.doi.org/10.1016/j.jcp.2012.11.034.

15. P. N. EDWARD and W. LARSEN, "Finite-Difference Approximations and Superconvergence for the Discrete-Ordinate Equations in Slab Geometry," *SIAM J. Numer. Anal.*, **19**, *2*, 334 (1982); http://dx.doi.org/10.1137/0719020.

16. J. D. DENSMORE and E. W. LARSEN, "Asymptotic Equilibrium Diffusion Analysis of Time-Dependent Monte Carlo Methods for Grey Radiative Transfer," *J. Comput. Phys.*, **199**, *1*, 175 (2004); http://dx.doi.org/10.1016/j.jcp.2004.02.004.

17. R. KONG and J. SPANIER, "A New Proof of Geometric Convergence for General Transport Problems Based on Sequential Correlated Sampling Methods," *J. Comput. Phys.*, **227**, 9762 (2008); http://dx.doi.org/10.1016/j.jcp.2008.07.016.

18. J. SHULTIS and W. DUNN, *Exploring Monte Carlo Methods*, Academic Press, Burlington, Massachusetts (2012).

19. T. URBATSCH and T. EVANS, "Milagro Version 2 An Implicit Monte Carlo Code for Thermal Radiative Transfer: Capabilities, Development, and Usage," LA-14195-MS, Los Alamos National Laboratory (2006).

AUTHOR QUERIES

Manuscript number: NSE16-36

A High-Order Low-Order Algorithm with Exponentially Convergent Monte Carlo for Thermal Radiative Transfer

Dear Jim E. Morel,

During the preparation of your manuscript for publication, the questions listed below have arisen. Please attend to these matters and return this form with your proof. Many thanks for your assistance.

AQ1— By "the above equation," do you mean Eq. (8) or the in-text equation in the previous sentence?

AQ2— Please define jks. Note that if you mean "jansky", the preferred symbol is Jy.